L2A+

Enhanced Aeolus L2A for depolarizing targets and impact on aerosol research and NWP

-

Description of the Algorithm Developments (ALGO)

Deliverable Item 03 [DI03]

(Final Version - FV)

Submitted to: Edward Malina (ESA)

	Name	Function	Date
Prepared by:	E. Proestakis	WP1000 – NOA	08/2024
	K. Rizos	WP3000 – NOA	08/2024
	A. Georgiou	WP4000 – NOA	08/2024
Approved by:	V. Amiridis	PI	08/2024

-

National Observatory of Athens (NOA)
Institute for Astronomy, Astrophysics, Space Applications & Remote Sensing (IAASARS)
Vas. Pavlou & I. Metaxa, 15236 Penteli, Greece
&
Leibniz Institute for Tropospheric Research (TROPOS), Leipzig, Germany
&
European Centre for Medium-Range Weather Forecasts
[ECMWF]
Reading, United Kingdom

[This page is intentionally left blank.]

Table of Contents

1. ESA-L2A+ DI03 – Overview.

This document consists the Deliverable Item 03 (DI03) – ALGO – Final Version (FV) submitted to the European Space Agency (ESA) by the consortium of the project "Enhanced Aeolus L2A for depolarizing targets and impact on aerosol research and NWP" (L2A+). DI03– ALGO reports on activities and developments related to L2A+ Work Package 3 (WP3000) – "Development of the L2A+ aerosol product" and Work Package 4 (WP4000) "Assimilation of L2A/L2A+ and application of WRF-L experiments". More specifically, DI03 – ALGO aims to document on the algorithms and methods used for the L2A+ retrieval and the data assimilation methodology and routines.

2. Introduction.

The European Space Agency's (ESA) wind mission, Aeolus, hosts the first space-based Doppler Wind Lidar (DWL) world-wide. Its scientific objectives are to improve Numerical Weather Predictions (NWP) and to advance the understanding of atmospheric dynamics and its interaction with the atmospheric energy and water cycle. Aeolus primary data product consists of profiles of horizontally projected line-of-sight winds from the surface up to about 30 km, and spin-off products are profiles of cloud and aerosol optical properties (e.g., Straume-Lindner et al., 2021). The Aeolus optical properties spin-off product (L2A; Flamentet et al., 2021) has been used to study smoke emissions, e.g., from 2019 Californian wildfires (Baars et al., 2021) and the early 2020 Australian fires, enhancement of volcanic ash forecasting systems and the impact of the Tonga eruption on tropospheric and stratospheric loads (e.g., Kampouri et al., 2021), and has been successfully experimentally assimilated in Copernicus Atmosphere Monitoring Service (CAMS) model C-IFS.

While the L2A product has a reasonable quality (see Baars et al., 2021, GRL, Paschou et al. 2021), its full potential for aerosol and cloud studies and for further improving NWP, has not been exploited. This is mainly because L2A is not provided separately for aerosol and cloud targets. Furthermore, the product is underestimated in terms of backscatter because the instrument measures only the co-polar part of the atmospheric backscattered return of the circularly polarized emitted beam (Paschou et al., 2021; Ehlers et al., 2022). Hence, in the case of strongly depolarizing targets (mainly desert dust particles and ice crystals), the signal measured at the detectors is strongly reduced with respect to non-depolarizing targets. Additionally, the expected atmospheric return signal in orbit is a factor of 2.5 to 3 lower than expected before launch due to lower laser output energies than originally intended (45–72 mJ) and decreased instrument transmission by about 30%, which has caused a lower SNR since mission start (Reitebuch et al., 2020).

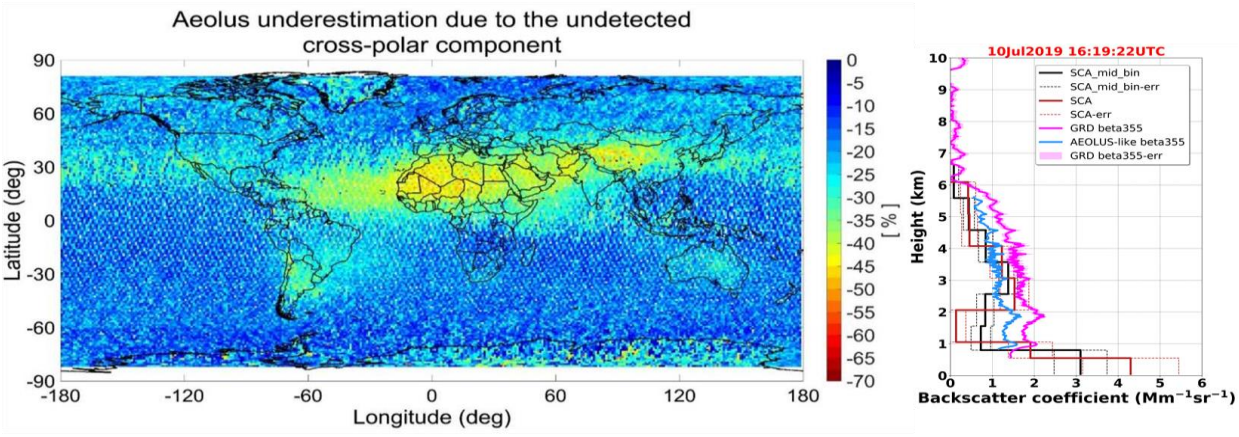

Figure 2.1: *Aeolus underestimation due to the missing cross-polar channel (a:) theoretical calculation; (b) observational evidence.*

There is a certain scope for delivering an enhanced L2A product based on a more detailed and robust classification, incorporating other data sources such as multi-sensor synergies or CAMS data. Furthermore, the potential of the extinction product should be further exploited as a constraint for the backscatter product for depolarizing targets, since the extinction is not affected by the missing cross-channel.

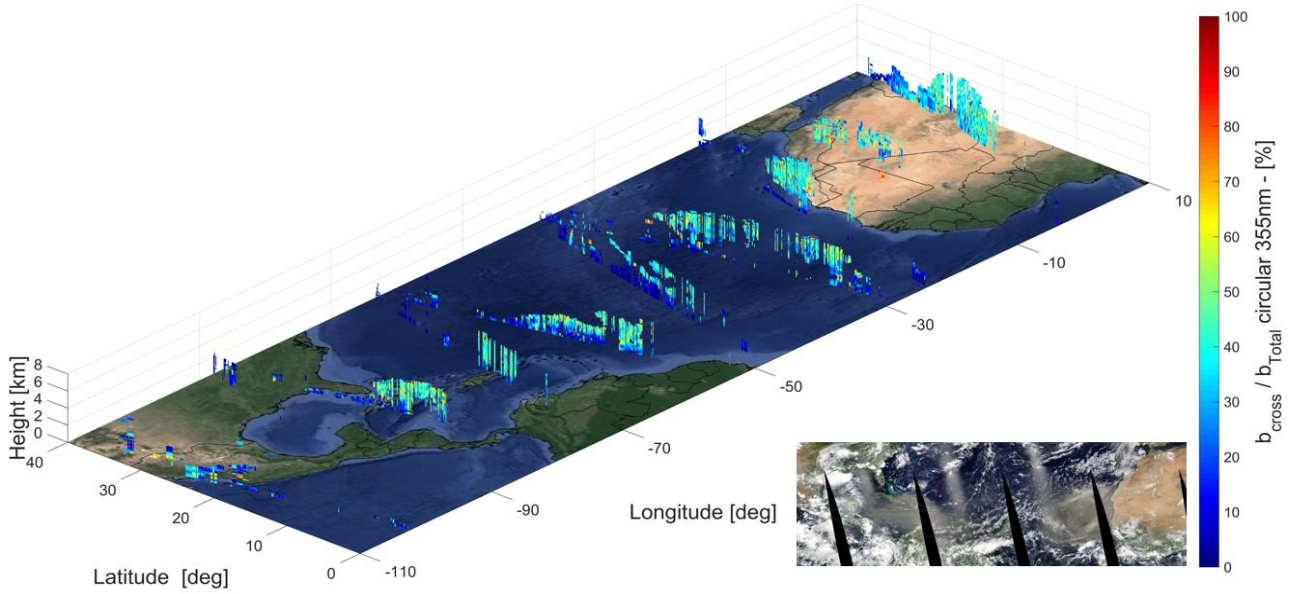

Figure 2.2: *Estimates of Aeolus L2A underestimation due to the missing cross-channel using the Aeolus-like profiles retrieved based on CALIPSO for the trans-Atlantic Godzilla dust event on the 23rd of June, 2020.*

ESA-L2A+ overarching objectives include the development of a refined Aeolus L2A aerosol product (L2A+), and accordingly test its applications for enhancing aerosol research, contributing to existing climate datasets. Furthermore, L2A+ aims at assessing the impact of the new product on aerosol assimilation towards improved dust transport modelling and for further enhancing NWP.
The following L2A+ individual objectives related to DI03 – ALGO are related to:

1) Objective 1: To develop a refined Aeolus aerosol optical product (L2A+), based on AEL-FM/AEL-PRO algorithms, geostationary AOD products, CAMS, and new AOD retrievals from the Aeolus itself (WP3000). The product will be thoroughly compared with L2A and validated against quality-assured measurements from the ESA-ASKOS/JATAC experiment in Cabo Verde (WP2000).
2) Objective 2: To examine the impact of L2A and L2A+ on aerosol assimilation and dust transport models (WP4000). Constraining aerosol loads through Aeolus assimilation is expected to improve dust emission fluxes over the Sahara Desert and transport simulations of the full particle size range (from fine to giant dust particles).

On the basis of L2A+, DI03 – ALGO aims to provide a consolidated view of the algorithms and methods used for the L2A+ retrieval and the data assimilation methodology and routines associated with the ESA-L2A+ overarching Objectives (1)-(5).

3. ESA-L2A+ WP3000: Development and validation of the L2A+ aerosol product.

3.1. Description of WP3000.

While the primary Aeolus aerosol product (L2A) has reasonable quality, its applicability in aerosol and cloud studies has not been exploited yet. The main reason is attributed to its deficiency to provide retrievals separately for aerosol and cloud targets. Furthermore, an underestimation of the backscatter coefficient is expected when the aerosol/cloud targets are depolarizing features (non-spherical particles); ALADIN provided only the co-polar part of the atmospheric backscattered return of the circularly polarized emitted light pulses. Towards overcoming the aforementioned inherent deficiencies, WP3000 aims to deliver an enhanced L2A product (with focus on dust) based on a more detailed and robust classification, involving multiple data sources such as multi-sensor synergies in conjunction with reanalysis numerical outputs and reference ground-based measurements. The new L2A product will be utilized on aerosol data assimilation schemes coupled with dust transport models with aim to improve Numerical Weather Prediction (NWP). The study period spans over the entire September 2021 when the JATAC/ASKOS campaigns took place in Cabo Verde. The region of interest refers to an extended tropical domain including the Sahara Desert and the Tropical Atlantic Ocean up to the Caribbean Sea. For the derivation of the enhanced L2A product, a series of processing steps has been designed which are presented in Figure 3.1.

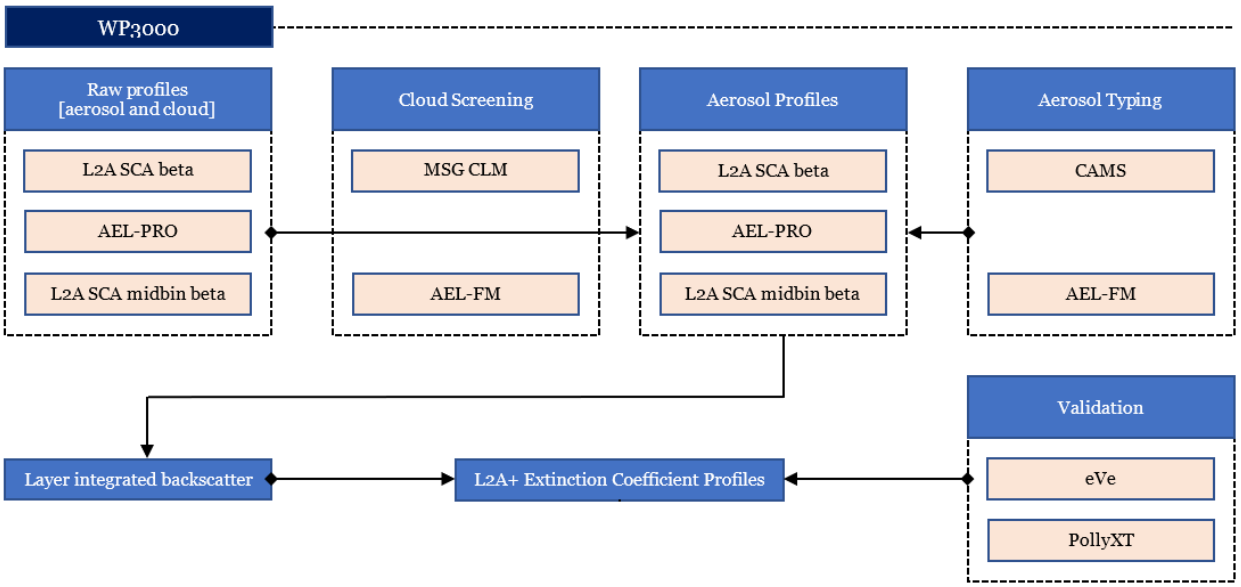

Figure 3.1: *A graphical presentation of the WP3000 processing steps.*

L2A+ starting point consists of the raw Aeolus L2A retrievals prior processed using a synergy of filtering tools. In the first working step a rigorous filtering of the raw Aeolus L2A retrievals will be performed for the elimination of the cloud-contaminated profiles. This cloud-filtering methodology will be performed relying on the AEL-FM (Aeolus Feature Mask) product from the L2A processors II (originated from the developments for the forthcoming EarthCARE mission but adapted to Aeolus) and the MSG-SEVIRI (Meteosat Second Generation - Spinning Enhanced Visible and Infrared Imager) CLAAS-3 cloud dataset. Based on AEL-FM retrievals, the features of the probed atmospheric scene are classified either as clouds or as aerosols or as molecular (Rayleigh) atmosphere. Moreover, the MSG-SEVIRI CLAAS-3 cloud dataset is also utilized as an extra or optional cloud-filtering tool for selecting only the pure aerosol Aeolus L2A profiles. The next working

step focuses on the identification of the dust layers at the cloud-filtered Aeolus vertically resolved profiles derived from the previous step. At this point, CAMS reanalysis data are used for the assignment of aerosol typing under the absence of an aerosol classification scheme on the raw Aeolus L2A data. In the third working task, the L2A+ aerosol extinction profile will be retrieved by using the Aeolus L2A+ cloud-free backscatter values and an appropriate lidar ratio value for the dust aerosol layers. Before the final product being injected in the WP4000, an assessment of the new L2A+ extinction profiles will be performed in the final working step against the corresponding ground-based retrievals acquired by the eVe and PollyXT lidars, operated in the framework of the JATAC campaign.

In the next sections we will present all the processing steps that have been undertaken up until now as well as some preliminary results.

3.2. Cloud-filtering of the raw Aeolus L2A retrievals.

In the first phase, a rigorous filtering of the raw Aeolus L2A backscatter coefficients retrievals have been performed for the elimination of the cloud-contaminated bins. In order to achieve the optimum cloud screening, the raw Aeolus L2a retrievals provided at BRC level, are jointly processed with the AEL-FM (Aeolus Feature Mask) retrievals and the MSG-SEVIRI (Meteosat Second Generation - Spinning Enhanced Visible and Infrared Imager) CLAAS-3 cloud dataset.

3.2.1. Cloud-filtering methodology based on AEL-FM feature mask product.

At first, the implementation of the cloud screening methodology was based on the AEL-FM retrievals. It is worth mentioning that the AEL-FM feature mask does not separate between different particle types but instead, it detects areas of strong and weak returns or those associated with clear sky conditions (van Zadelhoff et al., 2023). Based on the AEL-FM retrievals, the features of the probed atmospheric scene are classified either as clouds or aerosols or as molecular (Rayleigh) atmosphere. These referenced categories of scatterers, as well as their respective sub-types, are defined relying on image processing techniques and their availability along the Aeolus track facilitates the selection of the cloud-free Aeolus bins on the raw L2A profiles. In Table 3.1, the features that are categorized in the AEL-FM feature mask product are listed. In the first column, the main output of the AEL-FM feature mask product is given and corresponds to a feature detection probability index with values ranging from -3 to 10 and the second column presents how these indexes are defined. Based on the definitions, clear-sky conditions labeled with feature index value 0 are associated with very low signals expected to originate from clear air while stronger signals with values between 6 and 10 are most likely to have originated from liquid or optically thick ice clouds. Additionally, feature retrievals labeled with index value -3 are associated with signals directly affected by the surface.

Table 3.1: *Aeolus feature-mask features' definition. The first column provides the feature detection probability index ranging from -3 to 10. The second column shows the definition of each index.*

Index	Definition
10	Clouds
9	Most likely clouds
8	Very likely clouds or aerosols
7	More likely clouds or aerosols
6	Likely clouds or aerosols
5	Expected low altitude aerosol
4	Unlikely clouds or aerosol
3	Likely only molecules

2	Very likely only molecules
1	Most likely only molecules
0	Clear sky
-1	Fully Rayleigh attenuated
-2	No retrievals
-3	Surface data

Since the AEL-FM product is provided at the measurement level (~3 km), for the implementation of the cloud-screening procedure a conversion is required to be done in order to match the Aeolus' SCA horizontal and vertical resolution. The conversion process is illustrated in the figure below. In this example and due to space limitations only 3 BRC profiles are presented comprised with 3 measurements each. Depending on the L2A processor version, the total number of measurements accumulated in one BRC profile varies. According to the figure, in step 1 an example of the main output of the AEL-FM product is provided giving the feature detection probability indices with values ranging from -3 to 10. The conversion process (step 2) starts by putting the flag 'cloud' or "1" to the AEL-FM index values between 6 and 10 since according to the definitions given in Table 3.1 the associated returned signals are most likely to have been affected by clouds. The remaining AEL-FM index values from -3 to 5 were flagged with '0' since the associated returned signals are not likely to have been affected by clouds. This process gives us a binary matrix with the cloud-contaminated (1) and non-cloud-contaminated (0) measurements along the Aeolus track (step 3).

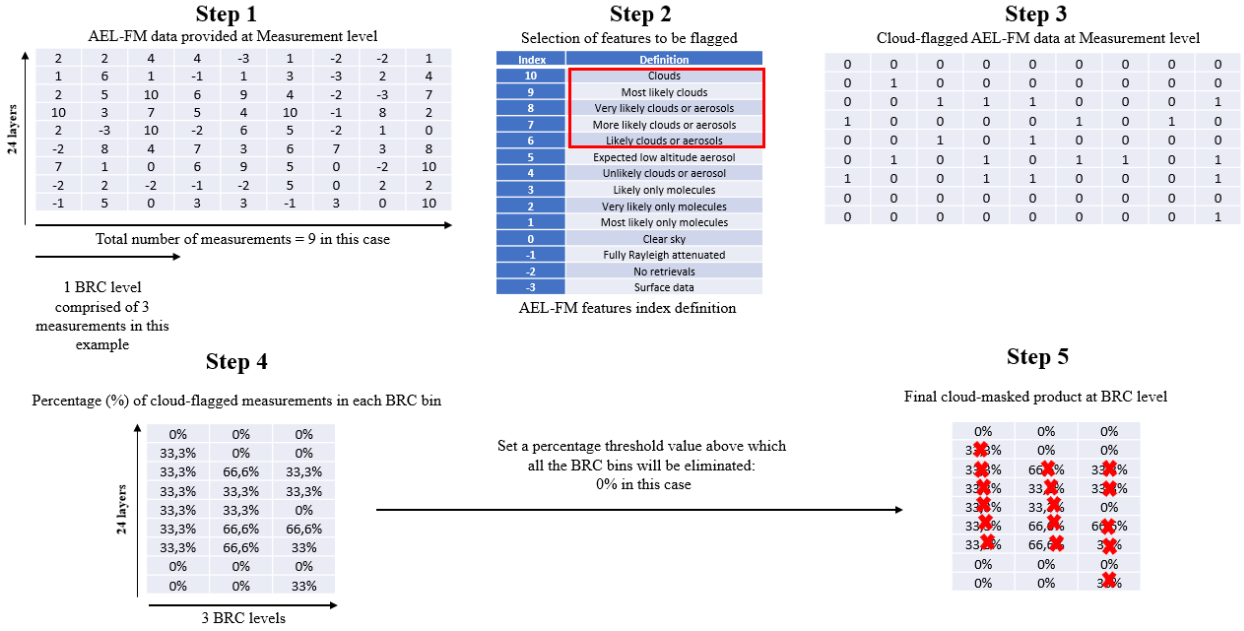

Figure 3.2: *A graphical illustration of the cloud-filtering methodology using the AEL-FM feature mask product.*

Then, in the next step (step 4) for each BRC bin comprised of three measurements each in this example, the total percentage of cloud-flagged measurements was computed. Based on the converted AEL-FM product (at the Aeolus' BRC level) giving the total percentage of "cloud-flagged" measurements for each BRC, the observations with values exceeding a threshold value (0% in this case) were considered as cloud-contaminated observations and the associated Aeolus SCA optical properties observations were eliminated (step 5). Following the aforementioned cloud-filtering process, the Aeolus L2A cloud-free backscatter profiles are derived.

For the first cloud-filtering methodology some preliminary results are presented for an indicative study case on 17th September 2021. Figure 3.3 shows the region of interest and the Aeolus satellite orbit path for the given case with the thick blue line indicating the ALADIN's measurement track.

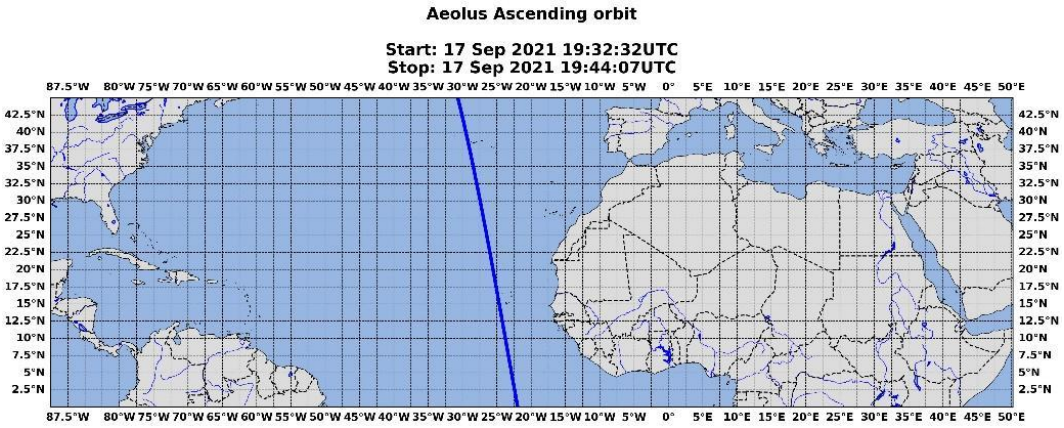

Figure 3.3*: Region of Interest and the Aeolus overpass (orbit id: 017790) on 17th September 2021.*

The cloud-filtering results for the specific Aeolus orbit are presented in the next figure (Figure 3.4). At first, the raw (unprocessed) Aeolus L2A profiles of the extinction and backscatter coefficient retrieved with the SCA algorithm are presented. Next, the primary AEL-FM feature-mask output along the Aeolus measurement track is shown where the classified features of the probed atmospheric scene can be observed. It can be seen that features associated with "strong" returns mainly attributed to clouds or high optically thick aerosol layers are colorized in brown and red respectively while those associated with the molecular atmosphere or clear sky conditions are colorized in green and cyan respectively. Then, for each BRC profile comprised of 30 measurements in this case the total percentage values of cloud-contaminated measurements are computed and presented in the next figure. Finally, based on the converted AEL-FM dataset given at the BRC level, the cloud-covered BRC bins exceeding 0% are detected and eliminated with the associated primary L2A Aeolus retrievals. In the last line of the figure the derived cloud-filtered extinction and backscatter SCA profiles are presented.

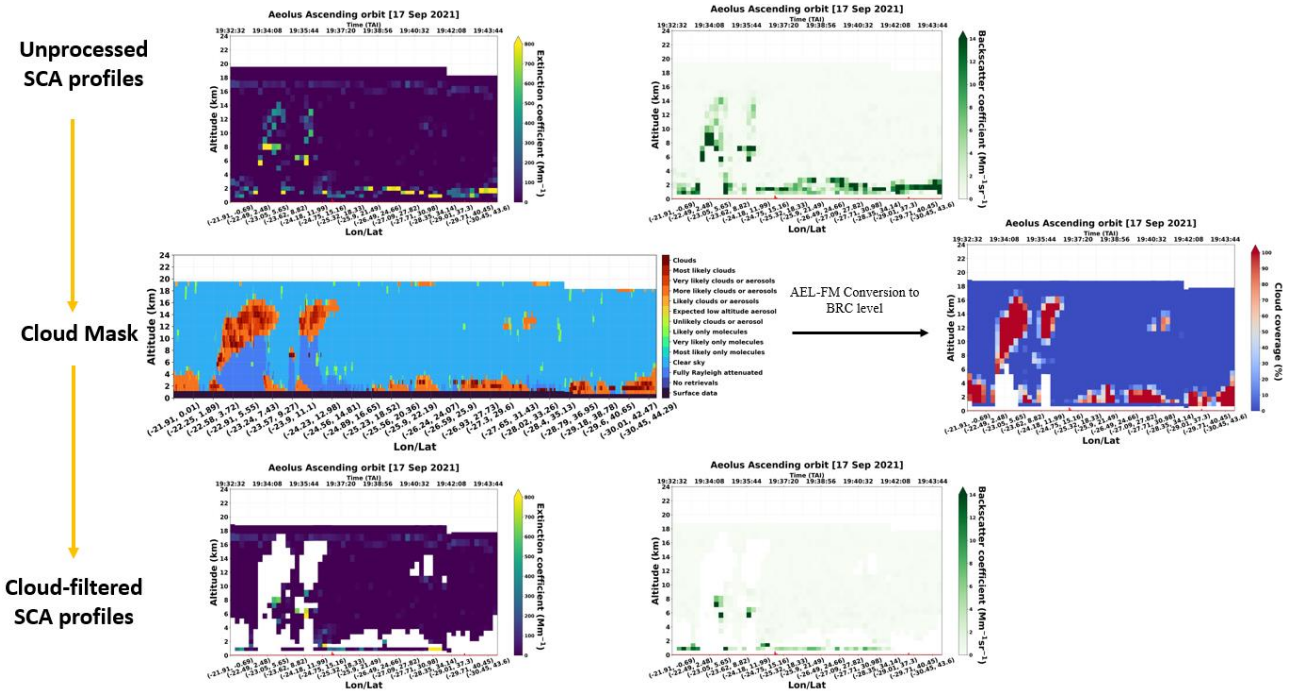

Figure 3.4: *Unprocessed profiles of L2A SCA backscatter coefficient; AEL-FM Feature Mask product at measurement level and cloud-covered (in%) BRC bins; Cloud-Filtered profiles of SCA extinction and backscatter coefficient for the Aeolus overpass of orbit id: 017790 on 17 September 2021.*

3.2.2. Cloud-filtering methodology based on MSG-SEVIRI CLAAS-3 cloud dataset.

For the second cloud screening process of the raw (unprocessed) Aeolus L2A profiles, the CLAAS-3 cloud dataset derived directly from the scene analysis of the MSG-SEVIRI (Meteosat Second Generation - Spinning Enhanced Visible and InfraRed Imager) imagery, will be processed. CLAAS-3 is the latest edition of CLAAS with previous editions documented in Stengel et al. (2014) and Benas et al. (2017). CLAAS-3 includes the following cloud properties: cloud mask/type, cloud top temperature/pressure/height, cloud thermodynamic phase, cloud optical thickness, cloud particle effective radius and cloud water path. Additionally, cloud droplet number concentration and cloud geometrical thickness are provided for liquid clouds. In cloud mask product, it is merely provided a categorization of the clear and cloudy pixels rather than a detailed information of clouds' macrophysical properties (i.e., cloud coverage), phase (i.e., ice, water, mixed) or types (i.e., low, middle, high). For the needs of the WP3000, the dataset has been provided for the whole study period of September 2021 from N. Benas - KNMI and S. Martin – DLR. An example of the MSG SEVIRI cloud dataset is provided in the figure below (Figure 3.5) for an indicative study case on 17th of September 2021 at 19.45 UTC where the grey and blue areas declare the cloud-covered and clear-sky areas. Additionally, an Aeolus ascending orbit on the specific date and time is also depicted.

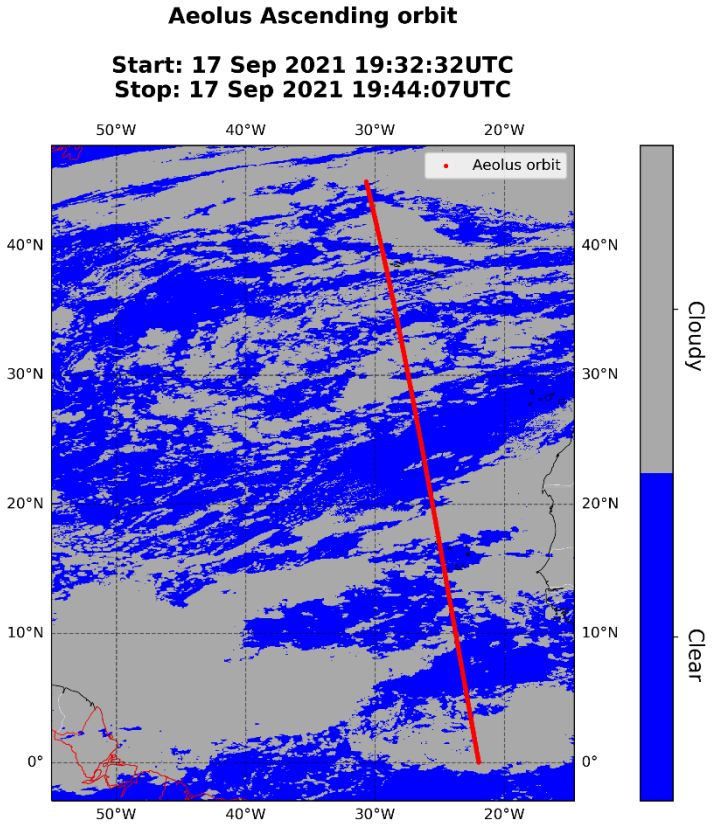

Figure 3.5: *SEVIRI CLAAS-3 cloud mask product for an indicative study case on 17th of September 2021 at 19.45 UTC and Aeolus orbit.*

For the identification of the cloud-contaminated Aeolus profiles, from the SEVIRI CLAAS-3 cloud mask dataset, the closest grid cells to the Aeolus ascending steps were selected. Then, for each grid cell with the flag "cloud" the associated Aeolus measurement step was flagged with the value of "1". Once the cloud-flagging process was completed, for each BRC profile the total percentage of cloud-contaminated measurements was computed. In the figure below the raw Aeolus L2A profiles of the extinction and backscatter coefficients retrieved with the SCA algorithm are presented. Accordingly, based on the MSG SEVIRI cloud dataset, the cloud-contaminated BRC profiles of the primary L2A Aeolus retrievals are detected and eliminated taking into account different test cases with different percentage values of cloud-covered BRC profiles.

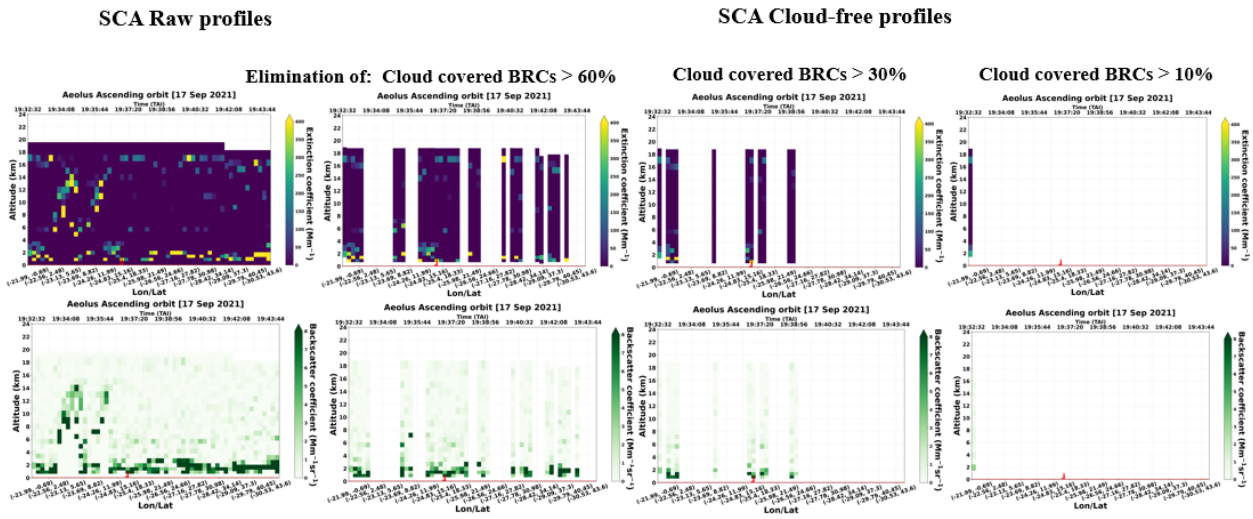

Figure 3.6: *SCA raw profiles of extinction and backscatter coefficients for a study case on 17th of September 2021. The associated cloud-free profiles for different percentage values of cloud-covered BRC profiles are given.*

It is worth mentioning that the whole cloud screening process based on AEL-FM and MSG SEVIRI datasets is still in the development stage and multiple cloud-filtering cases will be tested before the final cloud-free profiles are going to be used in the assimilation experiments of the WP4000.

3.2.3. Cloud-filtering implementation using the synergy of AEL-FM and MSG-SEVIRI.

For a more robust cloud-filtering of the raw Aeolus L2A retrievals, we also used the synergy of the AEL-FM feature mask product and SEVIRI cloud mask datasets, combining the already filtered Aeolus products from both filtering approaches described in sections 3.2.1 and 3.2.2. Figure 3.7 illustrates the pure aerosol profiles of the Aeolus L2A extinction and backscatter coefficients for the study case on 17th September 2021. It is worth reminding, that these cloud-filtered products have been derived after eliminating all the Aeolus BRC bins with cloud-contaminated measurements exceeding the 0% based on the rescaled AEL-FM product to the regular Aeolus's horizontal resolution (Figure 3.4) and all the BRC profiles with cloud-contaminated measurements exceeding the 60% based on the collocated cloud-contaminated pixels form SEVIRI cloud mask retrievals.

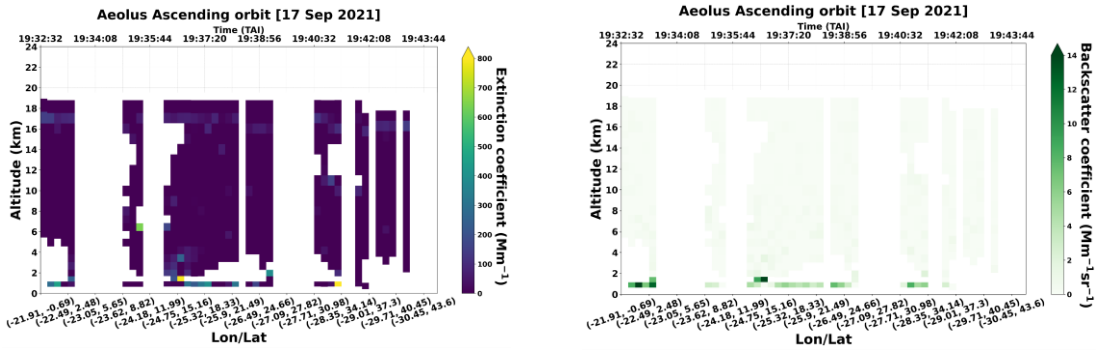

Figure 3.7: *SCA pure aerosol profiles of extinction and backscatter coefficients for a study case on 17th of September 2021.*

3.3. Aerosol typing using CAMS.

In this phase, the altitude ranges of the dust aerosol layers are defined on the derived cloud-free Aeolus L2A+ backscatter coefficient profiles from the previous working phase. Due to the absence of an aerosol classification scheme on the raw Aeolus L2A data, numerical outputs from the Copernicus Atmosphere Monitoring Service (CAMS) reanalysis (Inness et al., 2019) are implemented towards assignment of aerosol typing. The CAMS reanalysis dataset, produced by the Copernicus Atmosphere Monitoring Service, is the latest global reanalysis data set of atmospheric composition (AC) and it consists of 3-dimensional time-consistent AC fields, including aerosols, chemical species and greenhouse gases. The reanalysis methodology incorporates satellite with model data into a globally complete and consistent dataset using the European Centre for Medium-Range Weather Forecasts' Integrated Forecasting System (IFS) (Agustí-Panareda et al., 2023). The data set covers the period from January 2003 to June 2022 and it builds on the experience gained during the production of the earlier MACC reanalysis and CAMS interim reanalysis. For the production of the CAMS reanalysis data set, satellite retrievals of total column carbon monoxide (CO), tropospheric column nitrogen dioxide (NO2), aerosol optical depth (AOD); and profiles of ozone (O3) retrievals were assimilated (Inness et al., 2019). Compared with the previously produced CAMS interim reanalysis, the new ECMWF Atmospheric Composition Reanalysis (EAC4) has an increased horizontal resolution of ~80 km and it also provides an increased number of chemical species at a better temporal resolution (3-hourly analysis fields, 3-hourly forecast fields and hourly surface forecast fields) (Inness et al., 2019). For the present analysis, the total and dust aerosol component of CAMS model was used. Aerosol species are originally available in mass mixing ratio (kg/kg) and they include twelve prognostic tracers, consisting of three bins for sea salt grains of different sizes (0.03–0.5, 0.5–5 and 5–20 _m); three bins for dust (0.03–0.55, 0.55–0.9 and 0.9–20 _m); hydrophilic and hydrophobic organic matter and black carbon; and sulfate aerosols plus its precursor trace gas of sulfur dioxide (SO2) (Morcrette et al., 2009; Ryu & Min, 2021). Then, the total aerosol mass mixing ratio from CAMS was converted to mass concentration (μg/m3) using the following formula:

$$C_{PM10} = \left(\frac{SS_1 + SS_2 + SS_3}{4.3} + DD_1 + DD_2 + DD_3 + OM + BC + SU\right) * \left(\frac{p_m}{R_{spec} * T}\right) \quad (1)$$

where, SS1,2,3 refer to the sea salt particles of different size, DD1,2,3 to dust particles, OM to organic matters, BC to black carbon and SU to sulfates. Additionally, pm is the air density (kg/m3), T the temperature at vertical layer midpoint and Rspec =287.058 J/(kg · K) is the specific gas constant for dry air. In the above formula, the sum of the dust aerosol species (DD1,2,3), multiplied by the dry air concentration inside the parenthesis (p/R*T), calculates the mass concentration of dust aerosol species and it was used for the needs of the current methodology.

For the dust typing, some initial processing steps of CAMS reanalysis outputs have been undertaken. Specifically, for the study period, gridded data from CAMS were extracted for the entire Region of Interest (RoI). The data have a horizontal resolution of 0.5°, 60 hybrid sigma-pressure model levels on the vertical scale and a temporal resolution of 3h. An indicative study case is illustrated in Figure 3.8, presenting a Saharan dust outbreak on the 17th of September 2021, when dust-abundant air masses originating from N. Africa are crossing the Tropical Atlantic Ocean.

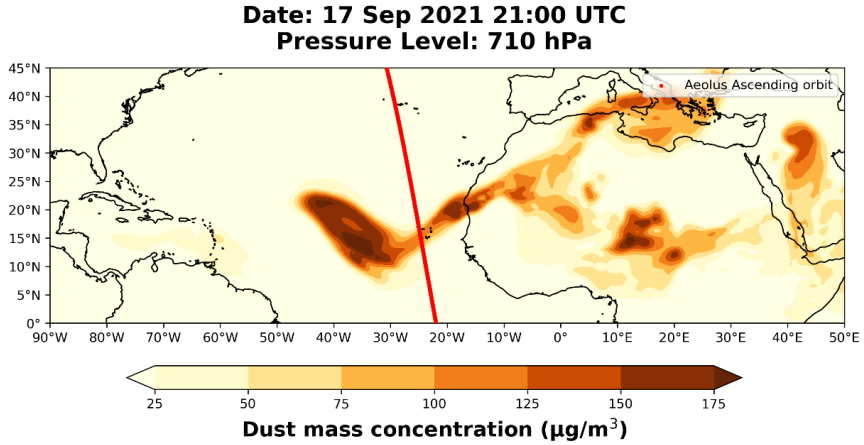

Figure 3.8: *CAMS dust mass concentration over L2A+ RoI for an indicative study case on the 17th September 2021. The red-coloured line presents the closest Aeolus orbit on the referenced time.*

In the next step, CAMS data were spatiotemporally collocated and vertically integrated in order to derive an Aeolus-type aerosol product from CAMS. An example of the rescaled CAMS products is given in Figure 3.9(upper panel) which illustrates the vertical profiles of the dust mass concentration along the specific Aeolus orbit (id: 017790) on the 17th of September 2021. We can clearly see specific BRC bins over the latitudinal band of 5°- 15°N up to 6km with elevated dust mass concentration values exceeding in many cases the value of 50 µg/m^3. The identification of the dust-contaminated layers was primarily based on the retrieved Aeolus-like dust mass concentration values selecting all the bins with concentration values higher than the median value of 1.3 µg/m3 . However, there would be a chance to wrongly select bins which may have been mixed with other aerosol types (sea salt, sulfates, etc.). To overcome this case, a second filtering parameter was also tested via the quantification of the dust-to-total aerosol mass concentration ratio value that gives the contribution of dust aerosols to the total aerosol mass concentration. Figure 3.9 illustrates also the vertical profiles of the dust-to-total aerosol mass concentration ratio values (in %) along the Aeolus measurement track. Then, the implementation of the dust-typing in the final step relied on both retrieved parameters, defining as dust-contaminated bins, those with dust mass concentration higher than 1.3 µg/m3 (median value) and dust-to-total concentration ratio higher than 50%. This filtering approach ensured the appropriate selection of bins with a strong presence of dust for the correction of the Aeolus's backscattered lidar signal.

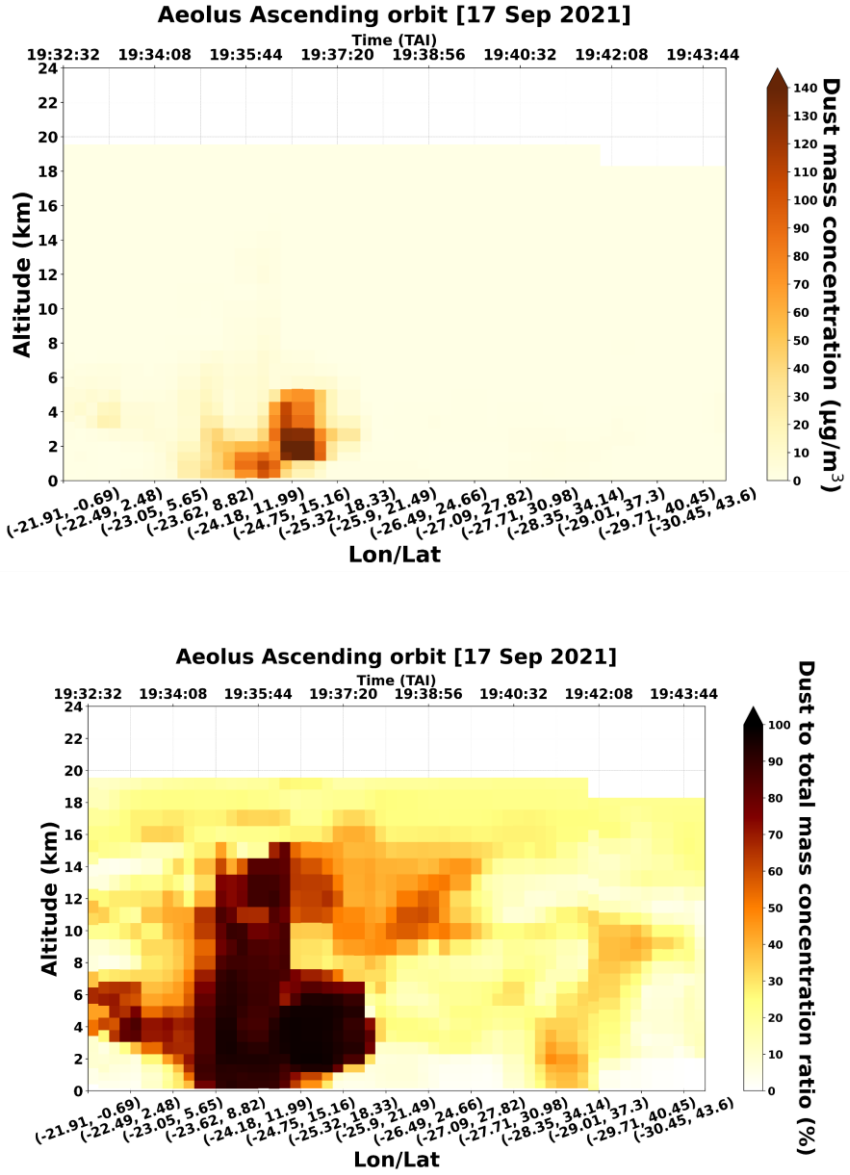

Figure 3.9: *Vertical profiles of CAMS dust mass concentration (upper panel) and dust-to-total concentration ratio (lower panel) along the Aeolus orbit (id: 017790) on the 17th of September 2021*

Figure 3.10 depicts the cloud-free Aeolus L2A extinction and backscatter profiles for the dust detected layers. In the next step, the focus will be given on these layers adjusting the missing cross-polar component of the backscattered lidar signal and reconstructing the Aeolus L2A extinction coefficient.

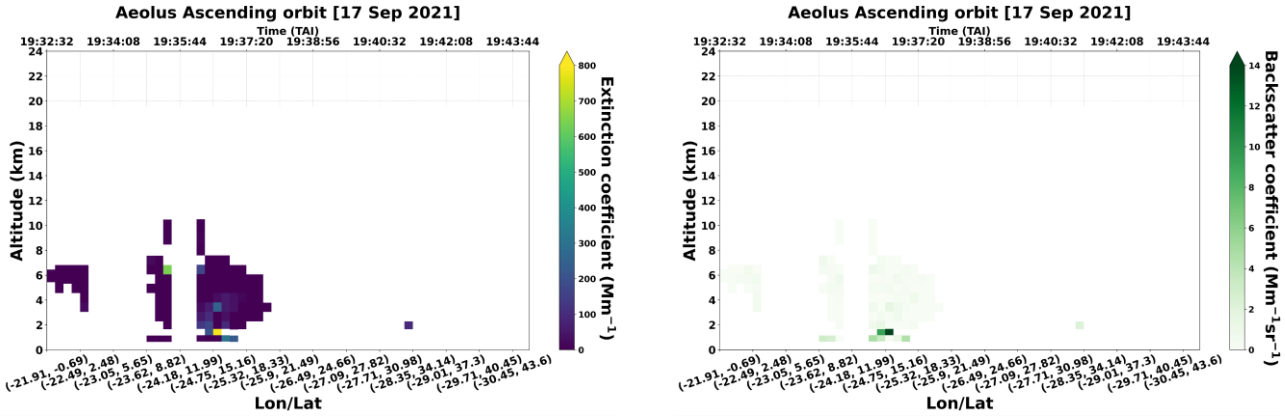

Figure 3.10: *SCA pure dust profiles of extinction and backscatter coefficients for a study case on 17th of September 2021.*

3.4. Retrieval of the L2A+ dust mass concentration.

In the current step, the mass concentration for dust aerosols was retrieved following a series of processing steps which included the retrieval of the Aeolus total backscatter coefficient accounting its missing cross-polar component, the computation of the L2A+ extinction coefficient using an appropriate value of the lidar ratio for the dust aerosols and finally, the conversion of the Aeolus L2A+ extinction coefficient to mass concentration using the POLIPHON method.

As has already been mentioned, ALADIN has been designed to measure the co-polar part of the backscattered lidar signals leading to an underestimation of the backscatter coefficient when non-spherical particles (dust, ice crystals, volcanic ash) are probed. To address this issue, a conversion between the co-polar part and total particle backscatter coefficient was implemented for the Aeolus' dust-contaminated bins identified in the previous step. The formula used for the conversion between the 355 nm co-polar part and total backscatter coefficient is the following:

$$\beta_{co,355}^{part} = \frac{\beta_{total,355}^{part}}{1 + \delta_{circ,355}^{part}} \quad (2)$$

where βco,355 is the Aeolus's co-polar part of the particle backscatter coefficient at 355 nm, βtotal,355 is the total backscatter coefficient at 355 nm and δcirc,355 is the circular particle depolarization ratio at 355 nm. However, the latter is not measured directly and it can be estimated indirectly using the linear depolarization ratio at 355 nm as follows:

$$\delta_{circ,355}^{part} = \frac{2\delta_{linear,355}^{part}}{1 - \delta_{linear,355}^{part}} \quad (3)$$

where δlinear,355 is the linear depolarization ratio at 355 nm. Floutsi et al. (2023) provide an experimental data collection (DeLiAn) of aerosol-type-dependent optical properties which includes the particle linear depolariation ratio, the lidar ratio and the Angstrom exponent obtained by lidar

systems during different field campaigns and at different locations over many years. In the above formula, the linear particle depolarization ratio value of 0.244 for Saharan dust was used from the DeLiAn database to convert between the 355 nm linear depolarization ratio and 355 nm circular depolarization ratio. Then, the computed circular depolarization ratio value was implemented in formula 2 and the total backscatter coefficient at 355 nm was retrieved.

In the next phase, the L2A+ extinction profiles for dust aerosols were derived by multiplying the retrieved Aeolus total backscatter values with a lidar ratio value of 53.5 sr obtained by the DeLiAn database (Floutsi et al., 2023) for the dust aerosol layers.

In the final step, the L2A+ extinction profiles were converted to mass concentration profiles, based on the POLIPHON method. The method which is analytically described by Mamouri and Ansmann, (2017) started by converting the L2A+ extinction profiles to dust volume concentration using the following formula:

$$v_{\mathrm{d}}(z) = c_{\mathrm{v,d},\lambda} \times \sigma_{\mathrm{d},\lambda}(z), \tag{4}$$

where σd,λ is the particle extinction coefficient at wavelength λ, and cv,d,λ the extinction-to-volume conversion factor derived from the AERONET long-term observations (Ansmann et al., 2019). Finally, the mass concentration for dust aerosols is given by

$$M_{\mathrm{d}}(z) = \rho_{\mathrm{d}} \times v_{\mathrm{d}}(z), \tag{5}$$

with the dust particle density ρd of 2.6 g cm−3 and the dust volume concentration v_d.

In Figure 3.11 the Aeolus profiles of the total backscatter coefficient, the L2A+ extinction coefficient and the final dust mass concentration product are illustrated for an indicative Aeolus overpass on 17th September 2021.

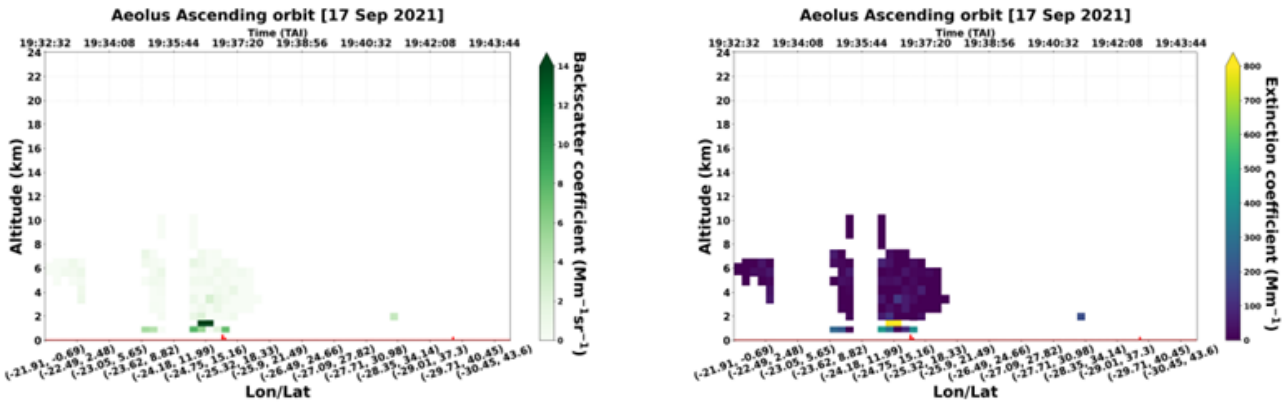

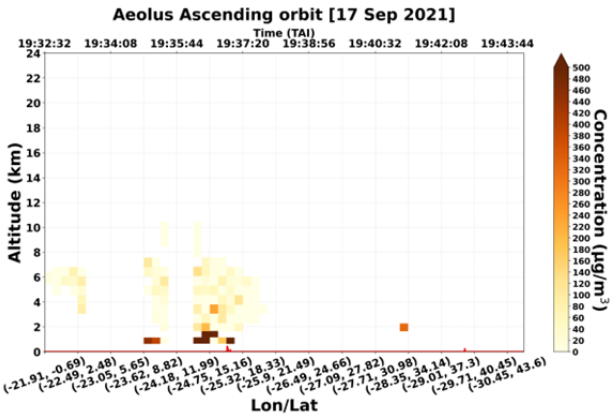

Figure 3.11: *SCA pure dust profiles of total backscatter coefficient, L2A+ extinction coefficient and mass concentration for the study case on 17th of September 2021.*

3.5. Validation of the L2A+ Aeolus product

In this part of the analysis, we evaluated the Aeolus L2A and L2A+ aerosol optical products, in particular the backscatter coefficient at 355 nm retrieved with three retrieval algorithms (SCA, SCA mid-bin and MLE algorithms) against ground-based measurements from eVe lidar collected during the ASKOS operations at Mindelo, Cape Verde during the summer months of 2021 and 2022 (July, September 2021 and June, September 2022). The process was performed considering the raw (unprocessed) Aeolus L2A co-polar backscatter profiles at 355 nm for each of the aforementioned algorithms (SCA, SCA mid-bin, MLE) and the quality-assured (QA) pure-dust total (L2A+) backscatter profiles at 355 nm after the adjustment of the missing cross-polar component. It is worth mentioning that only the quality-assured (cloud-free) ground-based measurements were used for the comparison process.

For the assessment analysis, we used the collocated Aeolus and ground-based retrievals. Specifically, for each ground-based measurement from the eVe lidar, the spatially and time closest Aeolus profile was selected for the validation process. An example of the assessment analysis is given in Figure 3.12, where the pure-dust Aeolus co-polar (L2A) and total (L2A+) backscatter profiles from the MLE algorithm are compared against ground-based aerosol backscatter profiles retrieved by eVe lidar for three indicative collocation cases on 10th, 17th and 24 September 2021. According to the results, it can be noticed that after the correction of the backscattered signal, the L2A+ backscatter profiles present a better agreement with ground-based measurements than L2A retrievals throughout the vertical range of the detected dust layer.

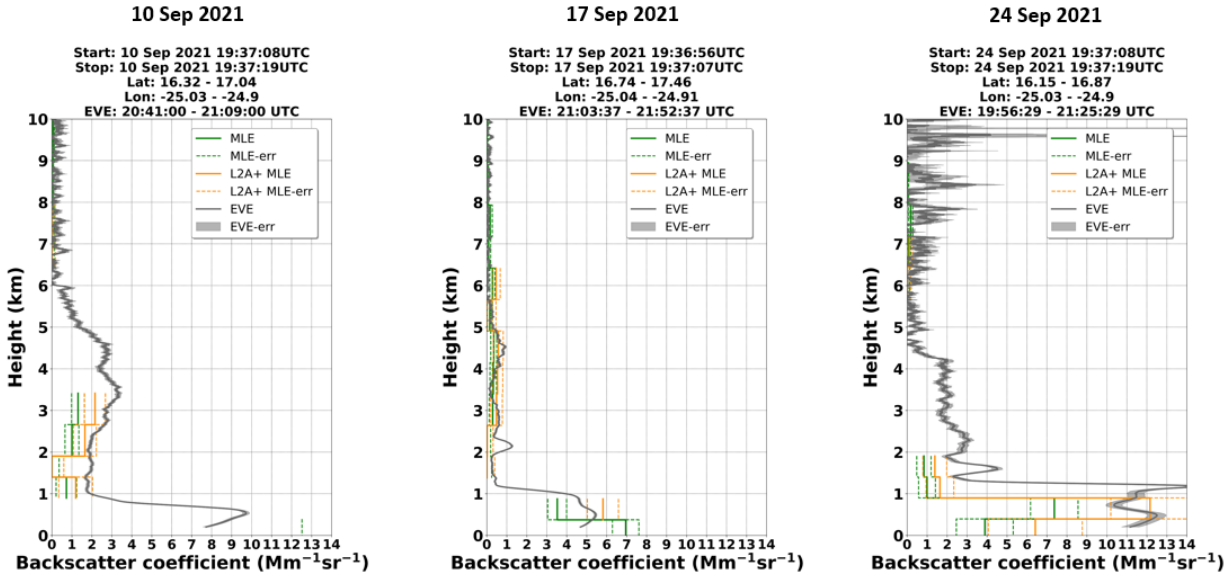

Figure 3.12: *Vertical profiles of the QA Aeolus L2A and L2A+ backscatter coefficient at 355 nm retrieved from MLE algorithm with the corresponding backscatter profiles acquired by eVe ground-based lidar.*

4. ESA-L2A+ WP4000: Assimilation of L2A/L2A+ and application of WRF-L experiments

4.1. Description of WP4000

The aim of this work package is to carry out Data Assimilation (DA) experiments to study the impact of joint Aeolus wind & aerosol information in a regional model, as well as determine the improvements brought by the development of the L2A+ product. As such, work was focused on setting up a regional dust transport model (WRF-CHEM) for assimilation (w/ NCAR DART) and incorporating the necessary tools and algorithms to assimilate Aeolus data. In this section we begin by describing our assimilation approach and how variables are transformed from model space to observation space and conclude by briefly describing the 3rd-party tools used and presenting their configuration.

4.2. Data Assimilation Overview

The overarching goal of any assimilation system is to estimate the probability distribution function (PDF) of the Earth system state at the initial time. To achieve this goal, a forecast is corrected with information from observations to provide a better estimate of the system state, called the analysis. This general idea is presented visually in Figure 1.

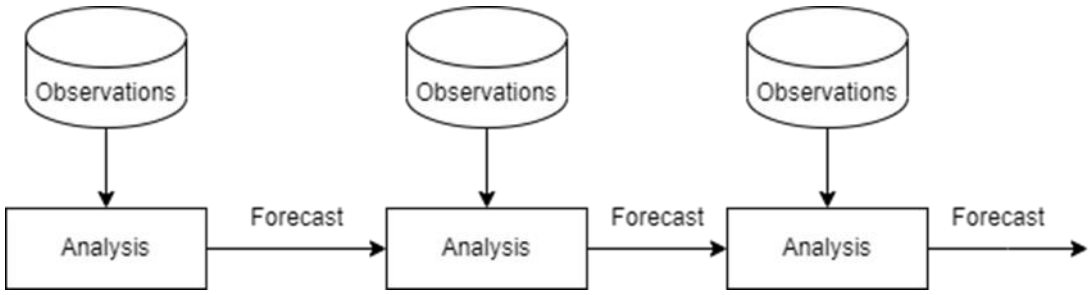

Figure 4.1: *A graphical presentation of the WP3000 processing steps.*

In L2A+, assimilation experiments are done using the Ensemble Adjustment Kalman Filter (EaKF, Anderson, 2001), as it is implemented in the Data Assimilation Research Testbed (DART, Anderson et. al., 2009)., In EaKF, the state of the atmosphere x_t (at time t) is assumed to have the conditional probability density function (PDF) $p(x_t \mid Y_t)$, where Y_t is the set of all observations of the atmospheric state at and before t. The initial PDF is sampled through an ensemble of n independent forecasts, which are then corrected by combining the distribution with each observation, in a Bayesian sense. The observation values must be directly comparable with the model state, and since this is rarely the case, EaKF uses observational operations to compute the model-equivalent observation for each real measurement, at the same location. EAKF comes in contrast with variational data assimilation methods in that the forecast error is estimated through the ensemble instead through a covariance model. EAKF has a disadvantage in that running the ensemble of forecasts is expensive in regards to computational resources but unlike variational DA methods, there is no requirement to have linear and adjoint versions of the model, nor the observational operators (Bannister, 2017). This greatly reduces the required development effort, an important aspect when dealing with new kinds of observations under a research context.

The algorithm is used as it is implemented in DART, thus interested readers are encouraged to refer to the original papers for detailed information. Nonetheless, figure 4.2 shows a high-level overview

of how EAKF works. At each timestep, the prior PDF of the atmospheric state is computed using the ensemble of independent forecasts. Then, this PDF is combined with the PDF of each observation to produce the posterior (or analysis) PDF of the atmospheric state.

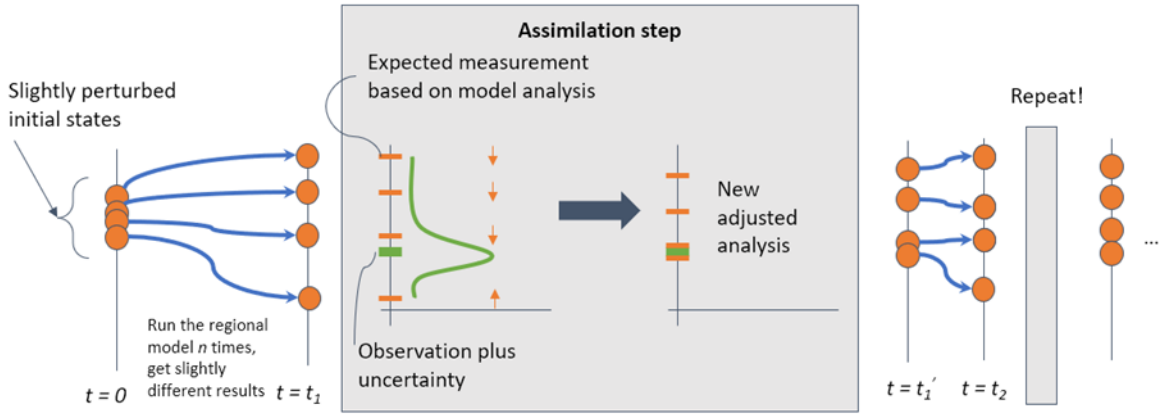

Figure 4.2: *A schematic showing how an Ensemble Kalman Filter data assimilation system operates.*

For each kind of observation, the appropriate operator must be developed to map the model state to observation space. For Aeolus, these are developed during the project and described in later subsections.

4.3. Experiment setup in L2A+.

In L2A+ the regional numerical weather prediction model used is WRF-CHEM (Advanced Research Weather version of the Weather Research and Forecasting coupled with Chemistry) (Grell et al., 2005; Skamarock et al., 2008), with the Georgia Institute of Technology-Goddard Global Ozone Chemistry Aerosol Radiation and Transport (GOCART) aerosol model and the Air Force Weather Agency (AFWA) dust emission scheme (LeGrand et al., 2019) for studying the life cycle of mineral aerosols. The WRF-CHEM model is coupled with the DART package in a cycling assimilation system.

In technical terms, the experiment setup requires running N independent forecasts with WRF-CHEM for a period of time (a cycle), at which point DART is used to assimilate Aeolus observations. The resulting analysis is used as initial conditions for starting the forecasts again for the next cycle. The ensemble size is 30 and the cycle length equals 6 hours.This procedure is shown visually in Figure 4.3.

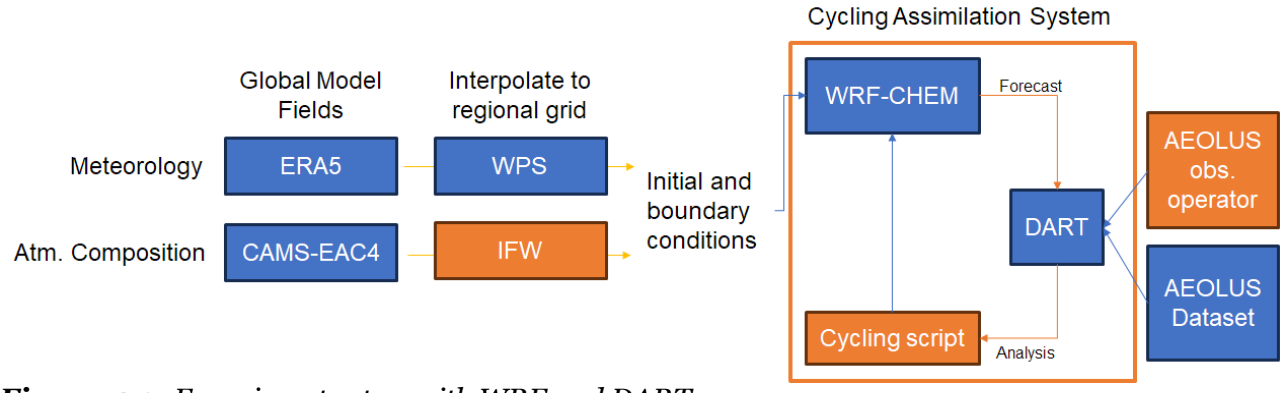

Figure 4.3: *Experiment setup with WRF and DART.*

The model domain is shown in Figure 4.4. It covers the general North Atlantic region, parts of Africa which are important for their dust emissions and parts of North and South America which are receptor points for dust transport. The ERA5 reanalysis (Hersbach et. al., 2020) is used as initial and boundary conditions for the meteorological fields, while for the dust fields the CAMS EAC4 reanalysis (Inness et. al., 2019) is used. While ERA5 is supported out-of-the-box by WRF-CHEM, the initial field interpolator (WPS) did not support CAMS EAC4 fields. An appropriate interpolator for global chemistry fields was developed during the course of the project, supporting CAMS EAC4 and CAMS Global Forecasts, while also being easily expandable to accommodate other global models. To map between the different dust size bins of CAMS EAC4 and WRF-CHEM's GOCART module, the overlap between each size bin was computed and from it, a set of linear coefficients was derived. The results of this technique as shown in Figure 4.5 and the resulting tool is available as an open-source project on Github

(https://github.com/NOA-ReACT/interpolator_for_wrfchem).

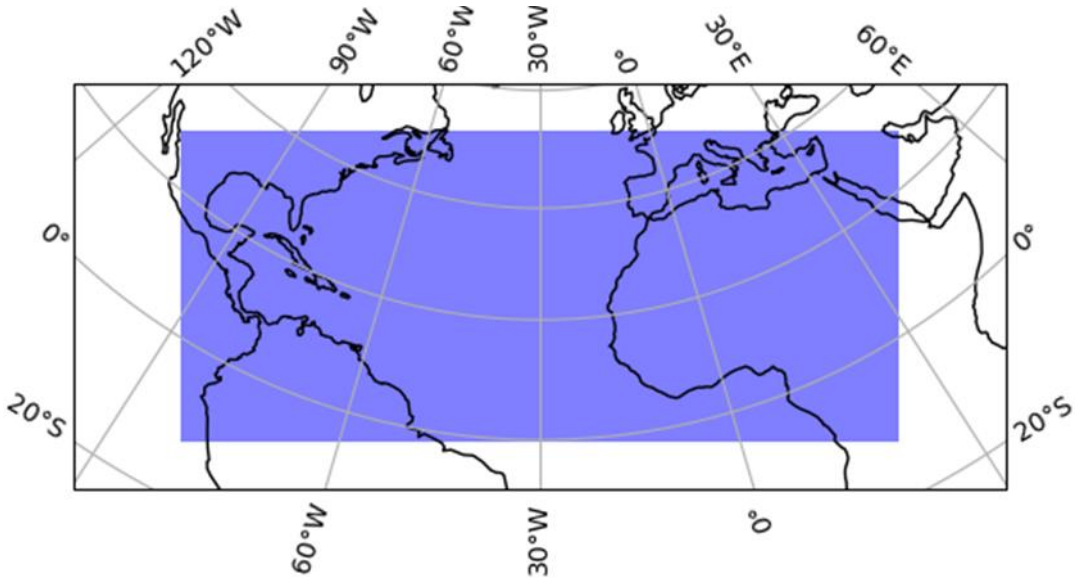

Figure 4.4: *Model domain shaded in blue.*

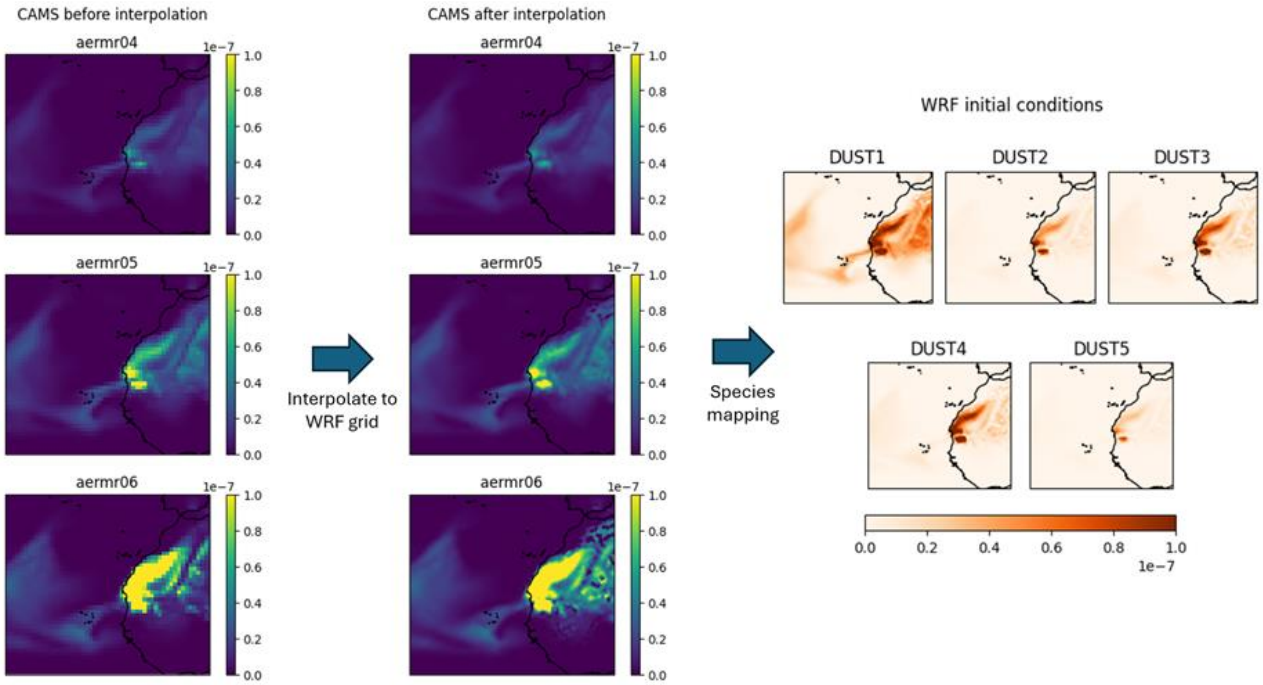

Figure 4.5: *Chemistry field interpolation steps, as implemented in Interpolator-for-WRFCHEM (https://github.com/NOA-ReACT/interpolator_for_wrfchem).*

To study the impact of Aeolus assimilation, a set of independent experiments were done, each having a different set of observations assimilated. The experiments are:

- CTRL: No data assimilation
- HLOS: Aeolus HLOS winds only
- HLOS/L2A: Aeolus HLOS and L2A
- HLOS/L2A+: Aeolus HLOS and L2A+

The addition of AOD assimilation from another instrument is currently under investigation, as it might help bring the total dust load closer to reality before Aeolus assimilation affects the vertical position.

4.4. Operators.

This subsection contains descriptions of the observational operators developed during the project, as required to enable data assimilation of Aeolus observations.

4.4.1. L2B Wind HLOS observations.

Aeolus measures horizontal line-of-sight (HLOS) wind speeds, which must be compared with the model's U and V wind vectors. The following observational operator is used (Šavli et al., 2018), where a is the azimuth angle, defined clockwise from north:

$$HLOS = U\ sin\ sin\ a\ + V\ cos\ cos\ a \tag{3}$$

4.4.2. L2A and L2A+ aerosol observations

The L2A and L2A+ products contain vertical profiles of aerosol optical properties, which must be compared to the dust mass concentrations in the model's state vector. To enable this, an operator was developed to compute aerosol extinction from model dust concentrations, based on the assumption of spherical dust and by using the Mie scattering code. For each dust size bin of the model, an Extinction Efficiency (Q, unitless) was computed, which can then be linearly combined with mass concentrations to yield the Extinction Coefficient (unitless):

$$Ext = \sum_{j}^{n} \frac{3M_j Q_j}{2\rho_j D_j}$$

where j is the dust size bin, M_j the mass concentration, ρ_j the particle density, and D_j is the effective diameter. The extinction efficiency parameter is dependent on the wavelength and it's been calculated for 355nm, 532nm and 1064nm, as to cover all common lidar systems.

List of Figures

List of Tables

Table	Description
Table 3.1	Aeolus feature-mask features' definition. The first column provides the feature detection probability index ranging from -3 to 10. The second column shows the definition of each index.

References

Agustí-Panareda, A., Barré, J., Massart, S., Inness, A., Aben, I., Ades, M., Baier, B. C., Balsamo, G., Borsdorff, T., Bousserez, N., Boussetta, S., Buchwitz, M., Cantarello, L., Crevoisier, C., Engelen, R., Eskes, H., Flemming, J., Garrigues, S., Hasekamp, O., … Wu, L. (2023). Technical note: The CAMS greenhouse gas reanalysis from 2003 to 2020. Atmospheric Chemistry and Physics, 23(6), 3829–3859. https://doi.org/10.5194/acp-23-3829-2023

Anderson, J. "An Ensemble Adjustment Kalman Filter for Data Assimilation." Monthly Weather Review, vol. 129, no. 12, Dec. 2001, pp. 2884–903. journals.ametsoc.org, https://doi.org/10.1175/1520-0493(2001)129<2884:AEAKFF>2.0.CO;2.

Anderson, J., Hoar, T., Raeder, K., Liu, H., Collins, N., Torn, R., Avellano, A., 2009. The Data Assimilation Research Testbed: A Community Facility. Bulletin of the American Meteorological Society 90, 1283–1296. https://doi.org/10.1175/2009BAMS2618.1Ansmann, A., Mamouri, R.-E., Hofer, J., Baars, H., Althausen, D., and Abdullaev, S. F.: Dust mass, cloud condensation nuclei, and ice-nucleating particle profiling with polarization lidar: updated POLIPHON conversion factors from global AERONET analysis, Atmos. Meas. Tech., 12, 4849–4865, https://doi.org/10.5194/amt-12-4849-2019, 2019.

Benas, N., Finkensieper, S., Stengel, M., van Zadelhoff, G.-J., Hanschmann, T., Hollmann, R., & Meirink, J. F. (2017). The MSG-SEVIRI-based cloud property data record CLAAS-2. Earth System Science Data, 9(2), 415–434. https://doi.org/10.5194/essd-9-415-2017.

C. Skamarock et al., 'A Description of the Advanced Research WRF Version 3', 2008, doi: 10.5065/D68S4MVH.

G. A. Grell et al., 'Fully coupled "online" chemistry within the WRF model', Atmospheric Environment, vol. 39, no. 37, pp. 6957–6975, Dec. 2005, doi: 10.1016/j.atmosenv.2005.04.027.

Hersbach, H., Bell, B., Berrisford, P., Hirahara, S., Horányi, A., Muñoz-Sabater, J., Nicolas, J., Peubey, C., Radu, R., Schepers, D., Simmons, A., Soci, C., Abdalla, S., Abellan, X., Balsamo, G., Bechtold, P., Biavati, G., Bidlot, J., Bonavita, M., De Chiara, G., Dahlgren, P., Dee, D., Diamantakis, M., Dragani, R., Flemming, J., Forbes, R., Fuentes, M., Geer, A., Haimberger, L., Healy, S., Hogan, R.J., Hólm, E., Janisková, M., Keeley, S., Laloyaux, P., Lopez, P., Lupu, C., Radnoti, G., de Rosnay, P., Rozum, I., Vamborg, F., Villaume, S., Thépaut, J.-N., 2020. The ERA5 global reanalysis. Quarterly Journal of the Royal Meteorological Society 146, 1999–2049. https://doi.org/10.1002/qj.3803

Inness, A., Ades, M., Agustí-Panareda, A., Barré, J., Benedictow, A., Blechschmidt, A.-M., Dominguez, J. J., Engelen, R., Eskes, H., Flemming, J., Huijnen, V., Jones, L., Kipling, Z., Massart, S., Parrington, M., Peuch, V.-H., Razinger, M., Remy, S., Schulz, M., & Suttie, M. (2019). The CAMS

reanalysis of atmospheric composition. Atmospheric Chemistry and Physics, 19(6), 3515–3556. https://doi.org/10.5194/acp-19-3515-2019.
J. L. Anderson, T. Hoar, K. Raeder, and N. Collins, 'Data Assimilation Research Testbed'. UCAR/NCAR - Computational and Information Systems Laboratory (CISL), 2004. doi: 10.5065/D6WQ0202.

J. L. Anderson, 'An Ensemble Adjustment Kalman Filter for Data Assimilation', Monthly Weather Review, vol. 129, no. 12, pp. 2884–2903, Dec. 2001, doi: 10.1175/1520-0493(2001)129<2884:AEAKFF>2.0.CO;2.

Morcrette, J.-J., Boucher, O., Jones, L., Salmond, D., Bechtold, P., Beljaars, A., Benedetti, A., Bonet, A., Kaiser, J. W., Razinger, M., Schulz, M., Serrar, S., Simmons, A. J., Sofiev, M., Suttie, M., Tompkins, A. M., & Untch, A. (2009). Aerosol analysis and forecast in the European Centre for Medium-Range Weather Forecasts Integrated Forecast System: Forward modeling. Journal of Geophysical Research, 114(D6), D06206. https://doi.org/10.1029/2008JD011235.

M. Šavli, N. Žagar, and J. L. Anderson, 'Assimilation of horizontal line-of-sight winds with a mesoscale EnKF data assimilation system', Quarterly Journal of the Royal Meteorological Society, vol. 144, no. 716, pp. 2133–2155, 2018, doi: 10.1002/qj.3323.

R. N. Bannister, 'A review of operational methods of variational and ensemble-variational data assimilation', Quarterly Journal of the Royal Meteorological Society, vol. 143, no. 703, pp. 607–633, 2017, doi: 10.1002/qj.2982.

Ryu, Y.-H., & Min, S.-K. (2021). Long-term evaluation of atmospheric composition reanalyses from CAMS, TCR-2, and MERRA-2 over South Korea: Insights into applications, implications, and limitations. Atmospheric Environment, 246, 118062. https://doi.org/10.1016/j.atmosenv.2020.118062

Stengel, M., Kniffka, A., Meirink, J. F., Lockhoff, M., Tan, J., & Hollmann, R. (2014). CLAAS: the CM SAF cloud property data set using SEVIRI. Atmospheric Chemistry and Physics, 14(8), 4297–4311. https://doi.org/10.5194/acp-14-4297-2014.

S. L. LeGrand, C. Polashenski, T. W. Letcher, G. A. Creighton, S. E. Peckham, and J. D. Cetola, 'The AFWA dust emission scheme for the GOCART aerosol model in WRF-Chem v3.8.1', Geoscientific Model Development, vol. 12, no. 1, pp. 131–166, Jan. 2019, doi: 10.5194/gmd-12-131-2019.

van Zadelhoff, G.-J., Donovan, D. P., & Wang, P. (2023). Detection of aerosol and cloud features for the EarthCARE lidar ATLID: the A-FM product. EGUsphere, 2023, 1–29.

[End of ESA-L2A+ DI03 – ALGO – FV]